Infrared Speckle Imaging at Palomar

A. M. Ghez, P. W. Gorham, C. A. Haniff, S. R. Kulkarni, K. Matthews, G. Neugebauer, and N. Weir

California Institute of Technology
Pasadena, California, 91125

ABSTRACT

We present diffraction-limited infrared images of three binary stars reconstructed using speckle imaging techniques. Three methods of recovering the objects' Fourier amplitudes are compared, Fourier deconvolution, projection onto convex sets, and CLEAN. The objects' Fourier phases are retrieved via bispectral analysis. We find that the quality of the final reconstructed images is a function of the percentage of the total bispectral volume utilized in the reconstruction procedure.

1. INTRODUCTION

Labeyrie's speckle interferometry has had much success in recovering diffraction-limited information on astronomical objects in the presence of atmospheric turbulence.[1] This technique, however, recovers only the object's Fourier amplitudes; the object's Fourier phases are lost. Nevertheless, in the past true images have been reconstructed with amplitude information alone.[2] These methods, however, are extremely sensitive to the noise level in the original data. Nowadays a number of techniques exist that have been developed to recover an object's Fourier phases from a set of short exposures, specklegrams.[3,4,5,6] We have implemented the technique of bispectral analysis, originally developed by Weigelt and his collaborators,[4,5] in order to retrieve diffraction limited phase information.

To utilize all the information contained in the bispectrum is a computationally intensive problem and requires a large amount of computer memory. This requirement in conjunction with the low signal-to-noise ratio (SNR) typical of optical data sets, for which speckle analysis was originally developed, led many groups to work with only a limited region of the bispectrum;[7,8,9] using only bispectral points near the axes because they have the highest SNR. In the low SNR regime ignoring the off-axis regions is sensible, because these regions contain relatively little useful information. In contrast the infrared speckle data that are presented in this paper have significantly high SNR throughout the bispectral volume. In this paper reconstructions of diffraction limited infrared images are presented, along with the results of an investigation of the relation between the volume the of bispectrum used with the quality of the reconstructed image and the comparison of three methods of amplitude recovery.

2. OBSERVATIONS

Observations were made at the f/415 Gregorian focus of the Hale 200-inch telescope on Palomar Mountain. The data was obtained with the Palomar infrared camera which contains a Hughes-Santa Barbara Research InSb hybrid array. The array has a rectangular format of 58x62 76 μm square pixels on a direct readout multiplexer having two readout amplifiers. Referred to the sky, the pixels are 0.055x0.055 arcsec in size and the array covers a field of 3.2x3.4 arcsec. The direct readout allows for shutterless operation, because, unlike a CCD, carriers are confined to each individual pixel. Each image is read in a raster fashion (see Fig. 1) at a rate of 18 μsec / pixel. Thus in time, the array is readout from the upper left pixel to the bottom right pixel, proceeding row by row. Since the "even" pixel in a row is read by one amplifier while the adjacent "odd" pixel is simultaneously read by the other amplifier the time to read an entire frame is 32 msec. The fact that the pixels are reset when read gives an almost 100% duty cycle at the expense of a temporal

skew in the frame of 32 msec from upper right to lower left. For these observations the frame exposure time was 100 msec and a narrow band filter ($\delta\lambda/\lambda = .012$) at 2.2 microns was used. Table I summarizes the observations.

Table I. Binary star observation parameters

Object	Mag(K)	#Frames
SAO 103106	5.8	320
SAO 86224	2.3	64
BS 8028	1.0	192

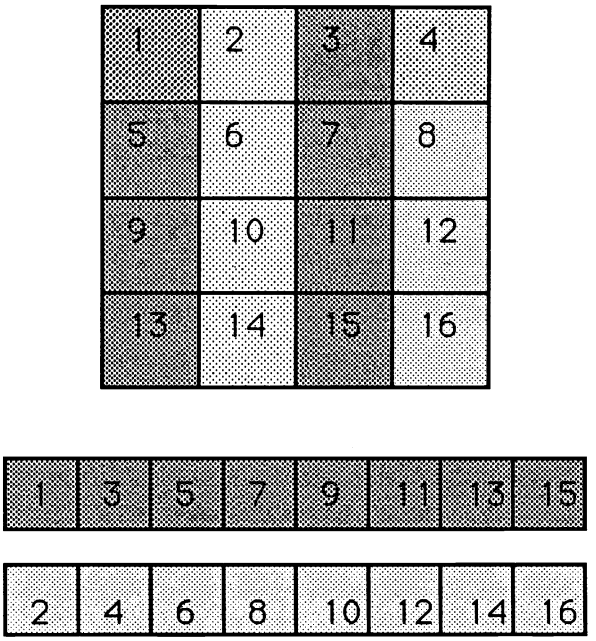

Fig. 1. A schematic drawing of the array readout sequence. Above is the two dimensional array, each pixel labeled as it is read in time. Below are the two one dimensional time series.

3. DATA ANALYSIS

The data reduction can be divided into a number of separate steps, which are listed below and discussed in the following subsections.

i. Removal of detector artifacts from the raw data
ii. Recovery of Fourier amplitudes
iii. Calculation of object and calibrator bispectrum
iv. Correction for systematic effects in the bispectrum
v. Recovery of Fourier phases
vi. Reconstruction of final image

3.1 Removal of detector artifacts

A worst case example of the raw data is shown in Fig. 2(a). This clearly demonstrates the need to remove detector induced artifacts; hereafter we will refer to this process as "scrubbing." An estimate of the images' background level is obtained using median filtered exposures of nearby blank sky. This is subtracted from the raw data. The nonuniformity of the pixels' sensitivity is

corrected for by flat fielding. The flat field used is the median filtered sky exposures, from which median filtered dark exposures have been subtracted. The dark exposures are taken with a cold shutter placed in front of the array, thereby measuring the detector's response in the absence of light. Dead pixels in the array, seen as two cracks and a number of individual pixels, and any cosmic ray events are interpolated over using the 8 nearest neighboring pixels. At this stage a ripple across the image becomes visible. This effect shows up clearly as a spike in the power spectrum of blank sky frames (see Fig. 3). The cause of this is related to the detector's readout electronic system. Since the array is readout into two channels a two-dimensional image can be decomposed into two one-dimensional time series. The power spectrum of these time series shows one dominant spike at a single temporal frequency, corresponding to 3 Khz. This feature is responsible for the spatial ripple seen in the image. This 3 Khz noise is removed by subtacting the appropriate sinusoid from the two time series, which are then recombined to form the two dimensional image. Currently, only this dominant readout artifact is removed, but as can be seen in Fig. 3, there are other frequencies that are corrupted at a lower level by the readout electronics. Nevertheless, once this scrubbing procedure is completed the speckle frames are free of detector artifacts down to the 1% level (Fig. 2.b).

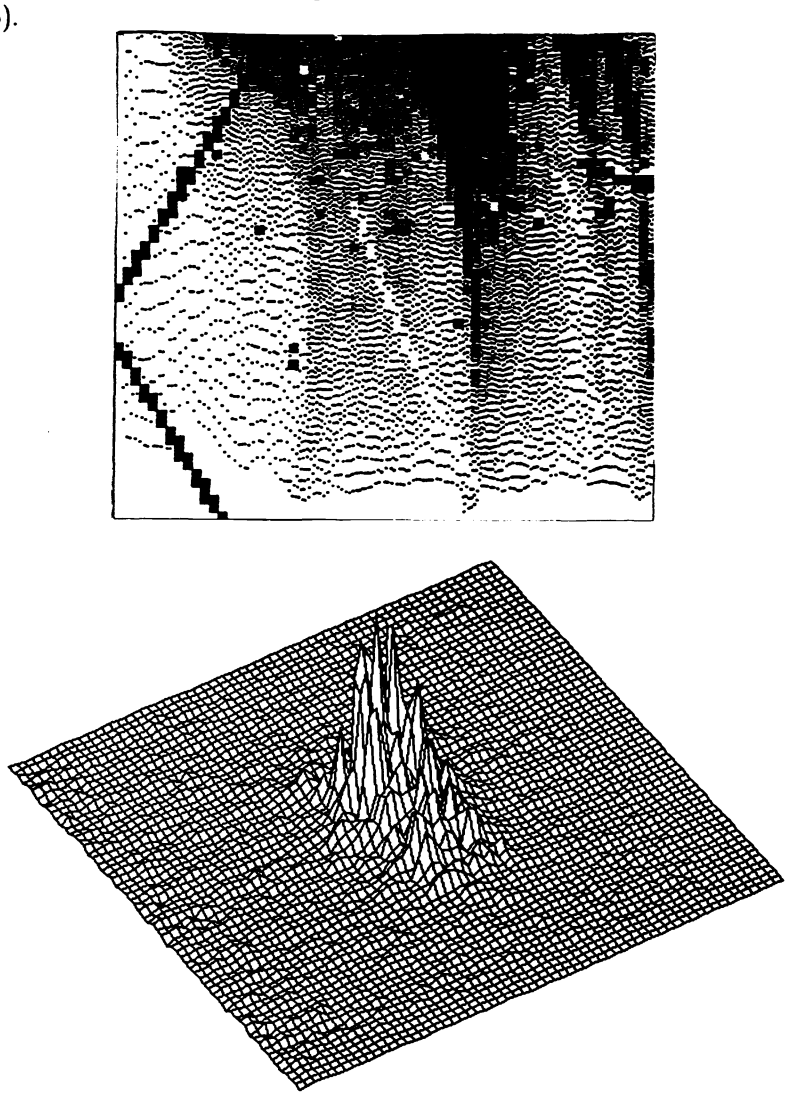

Fig. 2. (a) on the top shows an example of the raw data frame, and (b) on the bottom shows a "scrubbed" frame

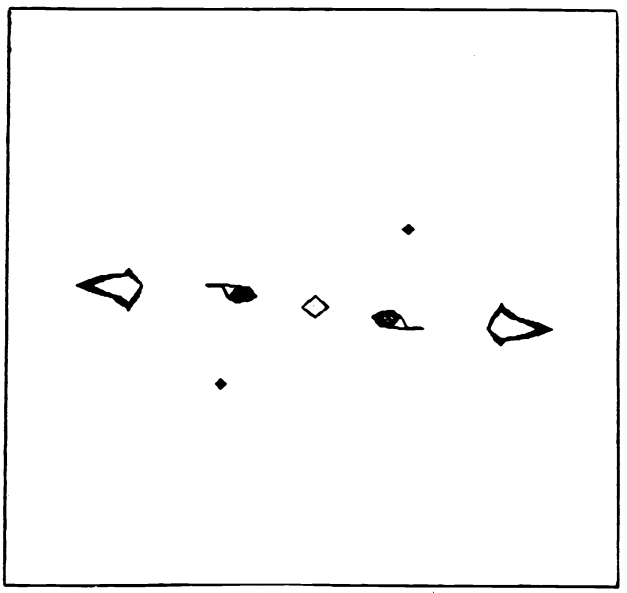

Fig.3 A power spectrum of blank sky

3.2 Amplitude recovery

Three methods for recovering the amplitudes of the object's complex Fourier spectrum have been compared: Fourier deconvolution,[1] projection onto convex sets,[10] and CLEAN.[11,12] The first method is the most commonly used one and recovers the obect's Fourier amplitudes by division of the ensemble average of the image power spectra, $< |J(\mathbf{u})|^2 >$, by the ensemble average of the power spectra of an unresolved source, $< |P(\mathbf{u})|^2 >$:

$$< |O(\mathbf{u})|^2 > = < |J(\mathbf{u})|^2 > / < |P(\mathbf{u})|^2 >$$

This technique has the drawback that the division process is unstable to noise in the calibrator power spectrum and will produce large fluctuations in the resulting spectrum. Because the noise level in a power spectrum tends to increase at higher spatial frequencies, the division estimate becomes poorer at higher spatial frequencies.

Projection onto convex sets is an iterative technique that applies constraints on an initial estimate of the true object's power spectrum, which is obtained by Fourier deconvolution as described above. This method iterates between the power spectrum and its Fourier equivalent, the autocorrelation function (ACF), applying constraints of positiviy and symmetry in both domains. The process proceeds until the changes produced in the power spectrum and ACF are below a set threshold. A more complete description can be found in Ebstein 1987.

An equivalent to the Fourier deconvolution may be done in the ACF domain using the CLEAN algorithm, which was originally developed for the deconvolution of the effects of irregular array spacings in aperture synthesis radio maps. CLEAN works by subtracting a fraction of the convolution function (the dirty beam) from the maximum point in the measured function (the dirty map), recording separately the position of the maximum and the amount subtracted. The

process is repeated until the maxima in the remaining dirty map fall into the noise or begin to appear outside the known region of emission. The list of maxima and their accumulated intensities are then convolved with a restoring "CLEAN" beam, and the residuals are added back into the map. In this application of CLEAN, the dirty beam is the ensemble-average calibrator ACF, and the dirty map is the ensemble-average image ACF. The resulting cleaned map is the true object ACF, from which the desired Fourier amplitudes are obtained.

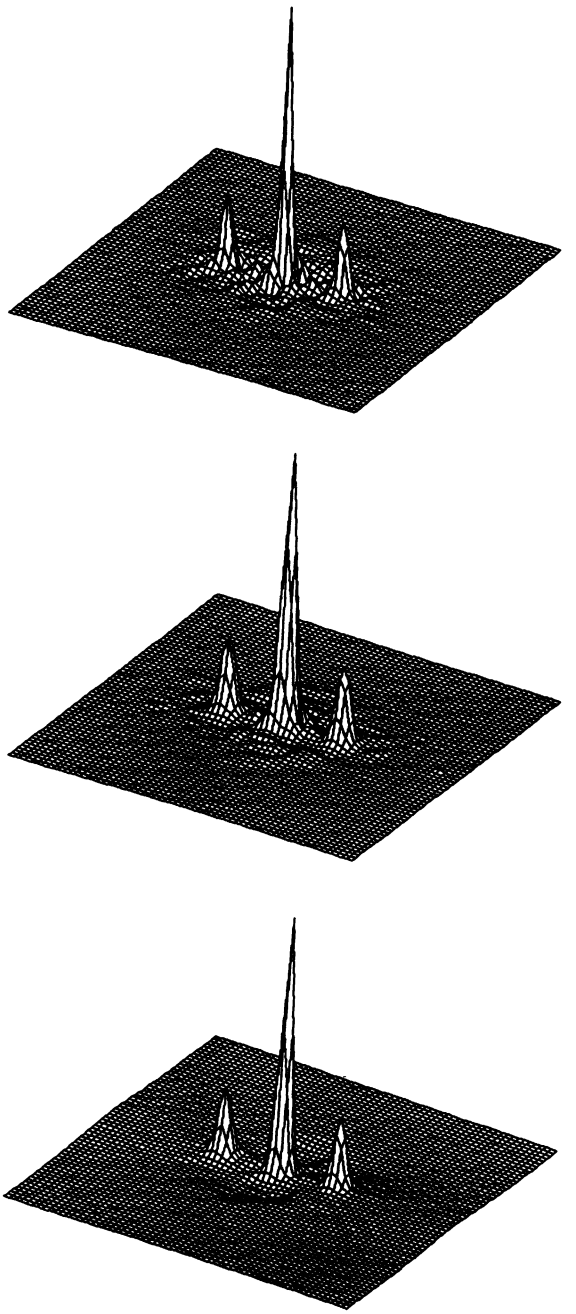

Fig. 4 A comparison of amplitude recovery schemes shown in the ACF domain. The top ACF was produced by Fourier deconvolution, the middle ACF was created with the projection onto convex sets, and the bottom ACF was produced with CLEAN.

Because of the simplicity of the objects' structure, it is possible to identify and characterize the systematic noise effects of the Fourier amplitude recovery processes. The results of the methods discussed above are presented in Fig. 4. The methods of projection onto convex sets and CLEAN introduce similar levels of noise to the object Fourier amplitudes, but the characteristics of this noise are different. High frequency noise located near the central region of the ACF is the dominant systematic noise effect in the results of both Fourier deconvolution and projection onto convex sets for our data, although the noise in the latter case is at a lower level. In contrast, the dominant systematic noise effect in the ACF recovered using CLEAN appears at low spatial frequencies. This effect is seen as a bowl in the final ACF and is probably due to a mismatch of seeing between the object and calibrator ACF's: this suggests that the dirty beam is not correctly approximated by the calibrator's ACF. Currently, the maximum level of noise is 1/80 of the maximum peak value in the ACF.

3.3 Phase recovery

The object's Fourier phases are recovered indirectly by measuring the bispectrum. The bispectrum is a triple product of the Fourier transform of the image measured at three spatial frequencies.[4]

$$B^3(\mathbf{u}_1,\mathbf{u}_2) = J(\mathbf{u}_1)J(\mathbf{u}_2)J(-\mathbf{u}_1-\mathbf{u}_2)$$

The crucial point to note is that the three spatial frequencies sum to zero, thereby forming "triangles". The phase of the bispectrum is thus equivalent to the closure phase of radio astronomy.[13,14]

$$\Phi_{123} = \phi_{\mathbf{u}_1}+\phi_{\mathbf{u}_2}+\phi_{-\mathbf{u}_1-\mathbf{u}_2}$$

Like the closure phase, the bispectrum phase can be shown to be immune to the type of phase errors introduced by the atmosphere.

As with any real system for taking speckle data, systematic biases are present in the raw data. One source of bias in our system is the detector readout electronics which corrupt certain spatial frequencies. Other sources of bias include telescope aberrations and the wide bandwidth employed. There are a number of procedures to correct for or remove "bad" bispectrum points, which are described in detail in Gorham et al.[9] Stationary biases, those that do not change from the time the source is observed to the time the calibrator is observed, that can be described by a transfer function can be corrected by subtracting the bispectrum phase of the calibrator from the image bispectrum phase. For our data, however, most of the biases are not removed by this method. It has proven more effective to remove these biases by eliminating those image bispectrum points for which the calibrator's bispectrum phase is statistically different from zero. This removes both stationary and nonstationary biases. The last step is to exclude image bispectrum points that have SNR < 1.

The bispectrum phases that remain are used to retrieve the object's Fourier phases. Because each bispectrum phase is a linear combination of three object Fourier phases, the measured bispectrum points define an overdetermined set of linear equations. There are two methods to solve for these phases. One technique is to solve for the phases recursively by initializing two of the object Fourier phases and directly solving for the remaining phases via linear combinations.[15,16,4] The other approach, which we have chosen, is to solve for the phases by a global least squares fit to the bispectrum.[9,14] This method avoids the propagation of errors in solving for the final object Fourier phases.

3.4 Image reconstruction

To prepare the final images the Fourier phases and amplitudes are combined and a direct Fourier inversion is preformed. This scheme effectively gives equal weight to the amplitudes and phases. This is not the optimal way to reconstruct images given that the amplitudes and phases are recovered independently and therefore have different final SNR. In the future, we hope to implement a scheme which appropriately weights the amplitudes and phases.

4. RECOVERED IMAGES

We have successfully reconstructed three binary star images, with 110 milliarcsec resolution (the maximum resolution of our system at 2.2 microns). These images are shown in Fig. 5 - 7 and their source parameters are given in Table II.

Table II. Binary star reconstruction parameters

Object	Sepn(mas)	PA(deg)	Dynamic Range
SAO 103106	550	264.5	40:1
SAO 86224	660	8	44:1
BS 8028	275	35	35:1

*dynamic range = ratio of the peak value to the highest spurious peak in the final map

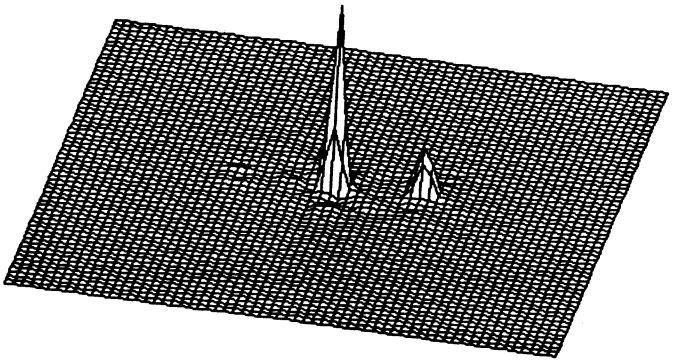

Fig. 5 Reconstructed image of SAO 103106

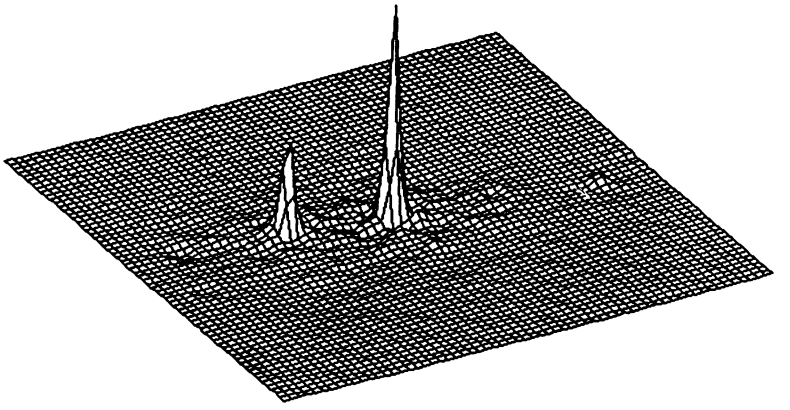

Fig. 6. Reconstruted image of SAO 86224

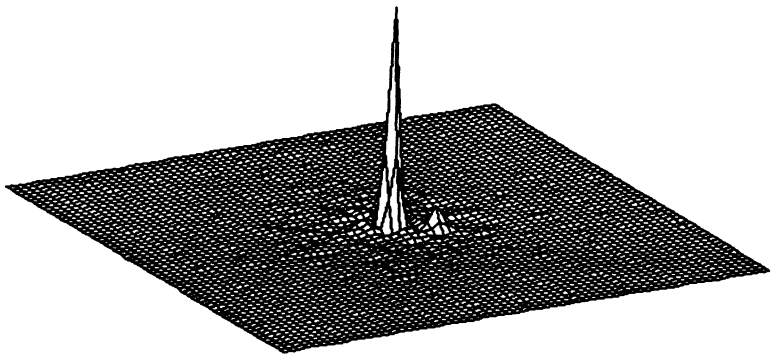

Fig. 7. Reconstructed image of BS 8028

In all of the reconstructions, the noise is dominated by systematic effects. For SAO 103106 (Fig. 5) and SAO 86224 (Fig. 6) ghost features appear at the point symmetric location from the secondary component. For the latter case there are also ghosts at the "harmonic" locations. The next significant noise features are artifacts of the amplitude recovery scheme. In the cases of SAO 103106 and SAO 86224, CLEAN was applied, and these images contain low frequency artifacts which appear as a low level bowl as discussed previously. The Fourier amplitudes for BS 8028 were obtained via Fourier deconvolution, and the dominant noise in the reconstructed image is the high frequency noise near the central region. The final type of systematic noise that we have identified is due to residual detector artifacts.

5. DYNAMIC RANGE VS. FRACTION OF BISPECTRAL VOLUME

All the infrared data that we have collected has high SNR points throughout its bispectral hypervolume. This is unlike photon-limited optical data for which the bispectrum typically has high SNR points only close to the axes.

We believe that there is valuable information to be gained from the off-axis region of the bispectrum. In order to investigate the useful information content of the off-axis bispectral regions, we examined how the quality of the image changed with the number of bispectrum points used in the reconstruction scheme. We have parameterized the quality of the image by the quantity dynamic range, which we define to be the ratio of the peak value to the highest spurious feature in the final image. We begin by using only the near-axis portion of the bispectrum to solve for the Fourier phases and produce an image. The near-axis bispectrum is obtained by constraining one of the spatial frequencies $\mathbf{u}_1$ to be small. In this case $\mathbf{u}_1$'s threshold is initially set to be one coherence length of the atmosphere, r_o. For our data set r_o is 30 cm, which corresponds to a frequency of three pixels. The number of bispectrum points used in the inversion is then increased by allowing the maximum value of $\mathbf{u}_1$ to increase at intervals given by r_o. The results of varying the fraction of the bispectrum used are shown in Fig. 8, and demonstrate the value of using the off axis regions in the reconstruction procedure. It should be noted that the dynamic range of the image of SAO 103106 is improved by almost a factor of three, although we are still limited by systematics, as is evident in the characteristics of the noise (bowls, ghosts, residual xy artifacts). However, by increasing the bispectrum volume included in the reconstruction these nonphysical artifacts are significantly reduced in size.

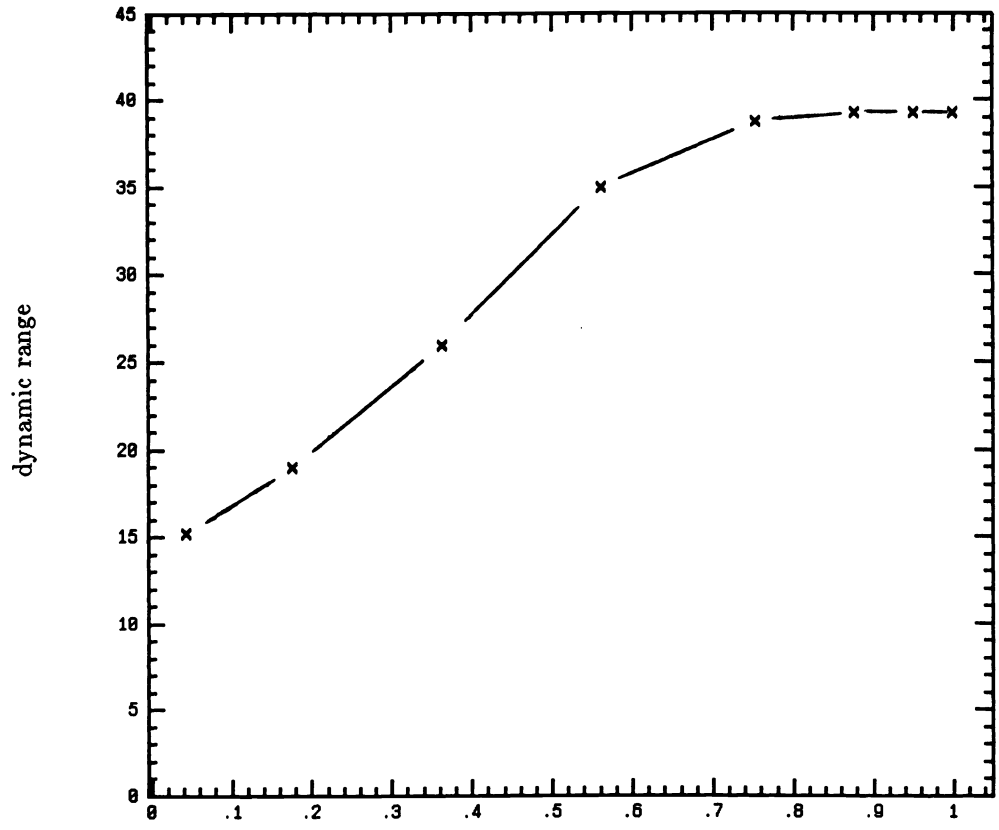

Fig. 8. Plot of dynamic range as a function of the fraction of the bispectrum used in the reconstruction procedure. This example shows the effect for the star SAO 103106.

As a way of estimating the ultimate quality of a reconstructed image, we have examined the background level away from the areas, such as the axes, that contain obvious systematics. Using the highest peak in these blank regions as an estimate of the limiting noise level, the expected dynamic range is about 600:1. We hope to be able to attain this level with more work on understanding the source of the systematics as well as improved reconstruction techniques.

6. CONCLUSIONS

We have successfully reconstructed three diffraction-limited infrared images of binary objects using bispectral analysis. The dynamic range of these images is approximately 40:1. We have shown that the quality of the reconstructed images improves by increasing the number of bispectrum points used, which indicates that there is indeed valuable information in the off-axis region of the bispectrum in the case of high SNR data. Further improvements in the reconstruction process are necessary to eliminate systematic noise effects. Using the background level to estimate the ultimate limiting noise level, we hope to be able to obtain images with dynamic range of about 600:1.

7. ACKNOWLEDGMENTS

We thank the W.M. Keck Foundation for their financial support, and the Concurrent Computing Center at Caltech for providing the NCUBE computer time for data reduction. We thank the staff of Palomar Observatory for their help with the observations. This work was supported in

part by DOE Grant No. DE-FG03-85ER25009, and NSF Grant No. AST8351736. S.R.K.'s research is supported in part by and NSF Presidential Young Investigator award, and the Alfred P. Sloan Foundation.

8. REFERENCES

1. A. Labeyrie, "Attainment of Diffraction Limited Resolution in Large Telescopes by Fourier Analysing Speckle Patterns in Star Images," *Astron. Astrophys.*, vol. 6, pp. 85-87, 1970.
2. J. R. Fienup, "Phase retrieval algorithms - a comparison," *Appl. Optics.*, vol. 21, pp. 2758-2769, 1982.
3. K. T. Knox and B. J. Thompson, "Recovery of images from atmospherically degraded short-exposure photographs," *Astrophys. J.*, vol. 193, pp. L45-L48, 1974.
4. A. W. Lohmann, G. Weigelt, and B. Wirnitzer, "Speckle masking in astronomy: Triple correlation theory and applications," *Appl. Optics,* vol. 22, pp. 4028-4037, 1983.
5. H. Bartelt, A. W. Lohmann, and B. Wirnitzer, "Phase and amplitude recovery from bispetra," *Appl. Optics,* vol. 23, pp. 3121-3129, 1984.
6. K. H. Hofmann and G. Weigelt, "Astronomical speckle masking: image reconstruction by cross triple correlation," *Appl. Optics,* vol. 26, pp. 2011-2015, 1987.
7. G. Weigelt, and B. Wirnitzer, "Image reconstruction by the speckle-masking method," *Opt. Let.*, vol. 8, pp. 389-391, 1983.
8. K. H. Hofmann, and G. Weigelt, "Speckle masking observation of the central object in the giant HII region NGC 3603," *Astron. Astrophys.*, vol. 167, pp. L15-L16, 1986.
9. P. W. Gorham, A. M. Ghez, S. R. Kulkarni, T. Nakajima, G. Neugebauer, J. B. Oke, and T. A. Prince, "Diffraction-limited imaging. III. 30 mas closure phase imaging of six binary stars with the Hale 5 m telescope," *A. J.*, vol. 98, pp. 1783-1799, 1989.
10. S. M. Ebstein, "Stellar speckle interferometry energy spectrum recovery by convex projections," *Appl. Optics,* vol. 26, pp. 1530-1536, 1987.
11. J. A. Hogbom, "Aperture synthesis with non-regular distribution of interferometer baselines," *Astron. Astrophys. Suppl.*, vol. 15, pp. 417-426, 1974.
12. P. W. Gorham, A. M. Ghez, C. A. Haniff, and T. A. Prince, "Recovery of diffraction-limited object autocorrelations from astronomical speckle interferograms using the CLEAN algorithm," *A. J.* (submitted), 1990.
13. F. Roddier, "Triple correlation as a phase closure technique," *Opt. Commun.*, vol. 60, pp. 145-148, 1986.
14. T. J. Cornwell, "Radio-interferometric imaging of weak objects in conditions of poor phase stability: the relationship between speckle masking and phase closure methods," *Astron. Astrophys.* vol. 180, pp. 269-274, 1987.
15. S. M. Ebstein, "Speckle imaging of galactic nuclei NGC 1068 and NGC 4151," *Ph. D. Thesis,* Harvard University, 1988.
16. O. von der Luhe, "Application of the Knox-Thompson method to solar observations," *Proc. ESO-NOAO joint workshop on "High angular resolution from the ground using interferometric techniques"*, NOAO, Ed. J. Goad, pp. 37-41, Oracle, 1987.